

Modelling Non-Uniform Bleed in Axial Compressors

S.D. Grimshaw, G. Pullan, T.P. Hynes

Whittle Laboratory

University of Cambridge

1 JJ Thomson Avenue

Cambridge, CB3 0DY, UK

Email: sdg33@cam.ac.uk

ABSTRACT

The coupling between the bleed system and the flowfield of a downstream compressor stage is studied using two approaches.

In the first, three-dimensional, full annulus, unsteady computations simulate the flow in a low speed research compressor with non-uniform bleed extraction. Comparisons with experimental data show that the flow prediction in the main annulus is accurate to within 0.005 of flow coefficient and 0.5° of flow angle. The CFD is then used to provide a description of flow within the bleed system itself.

In the second approach, a two-dimensional mean radius model, similar to that adopted by Hynes and Greitzer in previous work on compressor stability, is used to simulate the response of the compressor to non-uniform bleed. This model is validated against experimental data for a single stage compressor and despite the inherent assumptions (two dimensional flow and simplified compressor response) provides a satisfactory prediction of the flow for preliminary design purposes with orders of magnitude less computational cost than full 3D CFD. The model is then used to investigate the effect of different levels of bleed non-uniformity and of varying the axial distance between the bleed and the downstream stage. Reducing bleed non-uniformity and moving the stage away from the bleed slot are predicted to reduce the circumferential non-uniformity of the flow entering the stage.

INTRODUCTION

The bleed extraction from an axial compressor is typically circumferentially non-uniform. The principal cause for this is that, although the casing slot may be axisymmetric, the bleed flow is often distributed to other parts of the gas turbine via a finite number of off-take ducts. The result of this non-axisymmetric geometry is the imposition of a circumferential

static pressure distortion on the main annulus flow. Studies of uniform bleed have been performed using computations of compressors [1–3] and linear cascade experiments [4–6], as well as by the present authors using a rotating rig [7]. These studies show, that for typical design operating point bleed rates of 1% to 5%, there is limited spanwise redistribution of the flow due to bleed and a passage-averaged one-dimensional treatment is sufficient to model the compressor response. Non-uniform bleed has been investigated with annular cascade experiments [8, 9] and by the present authors [7]. Our tests demonstrated that the distribution of non-uniform bleed is linked to a reduction in compressor operating range and that this can be quantified using an approach similar to the DC_0 criterion that was developed to characterise inlet total pressure distortion [10].

The purpose of this paper is to address the question, “How should one analyse a compressor geometry with non-uniform bleed?” The answer to this question depends on the fidelity required at a given stage in the design process. We propose two strategies: for the final design, a high fidelity approach based on a full annulus unsteady CFD analysis of the compressor stage and bleed system; for preliminary design, a low fidelity approach based on a mean radius model that assumes the flow upstream of the compressor, including where the bleed is extracted, is linear and the compressor behaviour is input via a measured pressure-rise characteristic.

The paper is organised as follows: we first present the test compressor used to provide data to validate the modelling approaches. The CFD code and the meshing strategy used are then described and the results from the CFD calculations are compared with measurements and discussed. A qualitative description of the flow in the bleed system is developed based on the computations. Next we describe the approach, assumptions and specific elements that make up the low fidelity mean radius model. Finally, we show comparisons of the mean radius model predictions against test data, discuss the sensitivity of the model to assumptions, and investigate the effect of changing the bleed distribution and moving the downstream stage further away from the bleed extraction.

LOW SPEED COMPRESSOR RIG WITH BLEED

Experiments were performed with a one-stage, axial-flow, low-speed compressor with inlet guide vanes (IGVs) and a hub-to-tip radius ratio of 0.75, Grimshaw et al. [7]. Bleed air is extracted from the compressor through a bleed system which is located upstream of the stage. The compressor and bleed system design is typical of the rear stages of a land-based gas turbine and details are given in Table 1. Figure 1 shows the layout of the rig and the measurement stations referred to in this paper.

The bleed system has a small, axisymmetric plenum chamber, one off-take duct and bleed rate of 4.1%. This produces non-uniform extraction through the bleed slot which is measured using 16 pairs of static pressure tappings and stagnation pressure probes as described in [7]. The resulting distortion into the downstream stage causes a 3.0% increase in the stage inlet stalling flow coefficient as compared to the uniform bleed rate case.

Five-hole probe area traverses are performed with an automated traversing system. In all cases, each traverse is over one stator pitch and contains 21 equi-spaced pitchwise points and 21 radial points clustered towards the end walls. The relative position of the off-take duct and the traverse location is changed by moving the off-take duct to different circumferential positions.

Hub-to-tip radius ratio	0.75
Design $\phi = V_x/U$	0.43
Design $\psi = (p_2 - p_{01})/(\frac{1}{2}\rho U^2)$	0.48
Tip speed Mach number	0.23
Rotor $Re = (\rho V_1^{rel} c)/\mu$	1.6×10^5
Rotor tip gap	1.7% c_x (=0.4 mm)
Rotor blade count	58
IGV and Stator blade count	60
Casing diameter	0.51m
Plenum chamber ($\Delta x \times \Delta r$, volume)	$86 \times 10\text{mm}$, 0.0018m^3

Table 1: Data for low-speed compressor with bleed

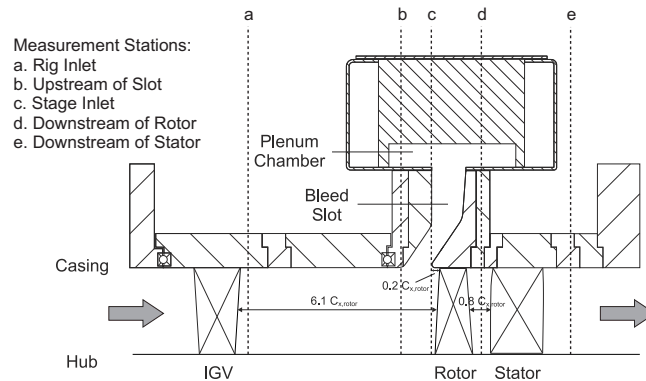


Fig. 1: Meridional view of test compressor showing measurement planes

HIGH FIDELITY APPROACH: FULL ANNULUS UNSTEADY CFD

The purpose of the CFD in the current work is twofold. First, to demonstrate the accuracy with which three-dimensional URANS calculations can model non-uniform bleed extraction and its effect on a downstream stage. Second, the CFD results allow the compressor and bleed system to be investigated in more detail than was possible in the experiments. There are several relevant pieces of work in which an approach, similar to ours, has been used to study non-uniformity on the lengthscale of the order of the circumference. Rosic et al. [11] investigate non-uniform extraction of steam for feed-heating from a steam turbine. They model a full annulus turbine with one extraction pipe using a RANS CFD solver and show that the non-uniform steam extraction associated with the discrete pipe causes non-uniform flow in the main blade passages. The work by Gunn and Hall [12] is the most recent of several studies which make use of full annulus URANS CFD to model the effect of inlet stagnation pressure distortion on compressor behaviour. Their simulation is validated against experimental results and is able to predict the detailed interaction between inlet distortion and a fan.

Methodology

The computations were performed using Turbostream [13], a structured multiblock URANS code based on the algorithms developed by Denton. The approach is finite-volume time marching, second order in space, with three levels of multigrid and a single step explicit time integration scheme. The solutions are second order accurate in time using Jameson’s dual time-stepping algorithm with 72 physical time steps per blade passing. A single equation Spalart-Allmaras turbulence model is used with adaptive wall functions and fully turbulent boundary layers.

The domain covers the geometry shown in Fig. 1 from upstream of the IGVs to downstream of the stage including the plenum chamber and off-take duct. In order to resolve the single off-take duct a full annulus grid is required (i.e. there are no rotational degrees of symmetry). This also allows the correct blade numbers to be modelled. The grid is generated using Autogrid, a commercially available mesh generator. The blade row meshes have an H-O-H topology and the tip gaps are modelled with two blocks which have an O-H topology. There are 121 spanwise points with 21 points in the tip gap. Values of y^+ are less than 8 on the blade surfaces. The plenum chamber and off-take duct are meshed with an O-H topology. The full mesh has approximately 250 million cells.

All computations were performed on graphics processing units (GPUs), allowing an order of magnitude reduction in runtime compared to running the same calculations on conventional processors. One operating point, with 3 rotor revolutions, required 100 hours on 48 GPUs.

Results

The full annulus CFD calculation is run at an annulus-averaged stage inlet flow coefficient $\bar{\phi}_{\text{stage}} = 0.43$, with a bleed rate of 4.2%. The solution considered here is time-averaged over 29 rotor blade passings, i.e. half a rotor revolution. In this section we will show passage-averaged data from the computed main annulus flow compared with experimental measurements; second, we plot computed contours of flow coefficient at each measurement plane and discuss the main annulus flow field; third, we provide plots of streamlines within the bleed system and a qualitative description of this flow.

Passage-averaged Analysis

In anticipation of the mean radius model to follow, we first present the passage-averaged behaviour of the compressor. In this way, the CFD and experimental data are reduced to a two-dimensional “mean-radius” framework.

Figure 2 shows comparisons between experimental measurements and CFD simulations of passage-averaged flow coefficient, flow angle and relative flow angle around the annulus and at different axial positions. At each measurement station the computed flow distribution provides a very good match to the rig data. The computed flow coefficient in all cases is predicted to within 0.005 (1.2% of $\bar{\phi}$) and the flow angle to within 0.5° .

Rig inlet

Figure 3 shows computed contours of flow coefficient at rig inlet. The flow coefficient in the main passage is increased in the region close to the circumferential position of the off-take duct and this redistribution is approximately uniform across the span. The circumferential variation of flow angle, shown in Fig. 2(a) is small (less than 0.5°) as expected at the location close to the IGVs and $5C_{x,rotor}$ upstream of the bleed slot.

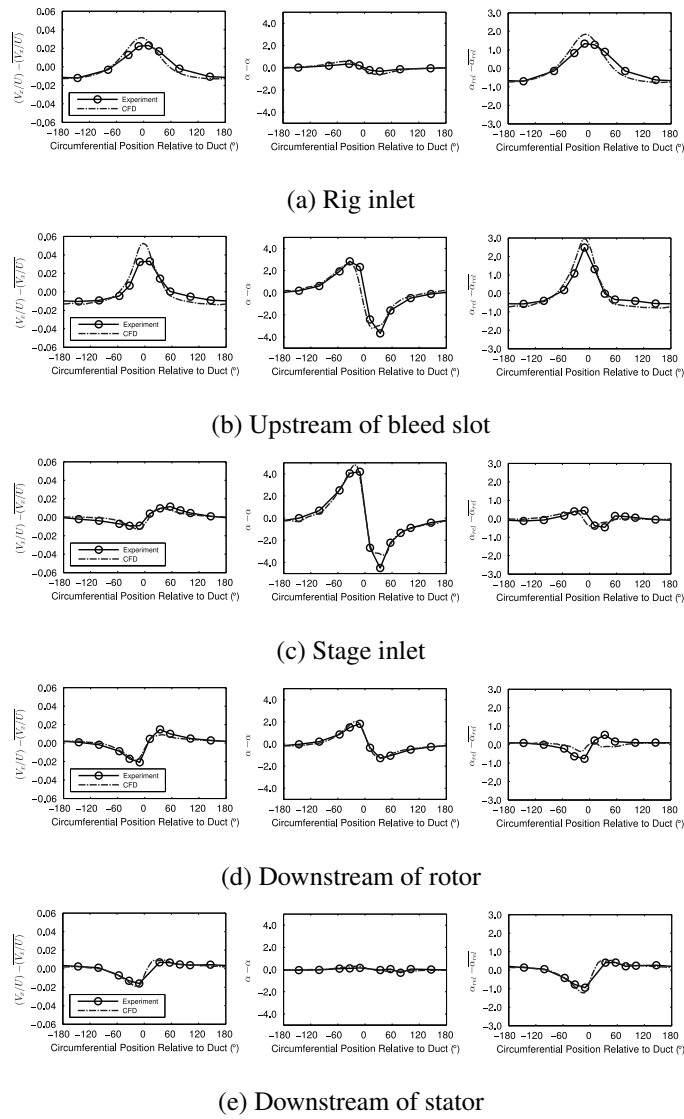


Fig. 2: Comparison of passage-averaged experimental data and model output downstream of stage, $\bar{\Phi}_{\text{stage}} = 0.43$

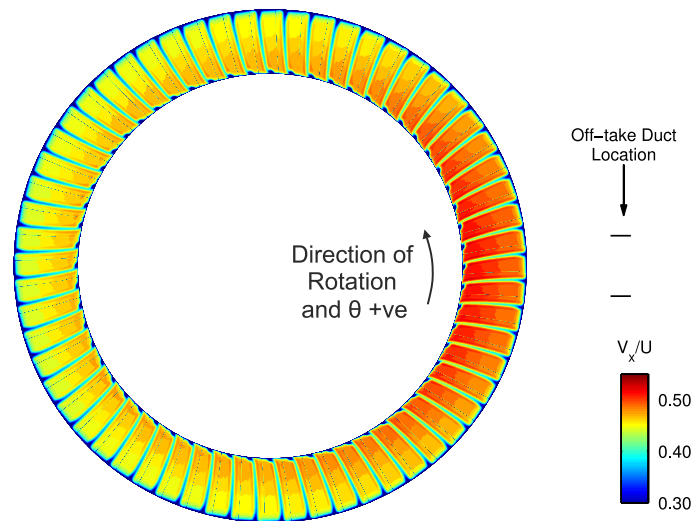


Fig. 3: Rig inlet, CFD calculated flow field. $\bar{\Phi}_{\text{stage}} = 0.43$, bleed rate = 4.2%

Upstream of bleed slot

Contours of flow coefficient upstream of the bleed slot are shown in Fig. 4. The flow coefficient is increased close to the circumferential position of the off-take duct, and particularly in the outer 30% of span. Figure 2(b) shows that the flow angle varies asymmetrically about the off-take duct location. This is due to the static pressure field created by the discrete off-take duct turning the streamlines in the flow towards the region of maximum bleed extraction.

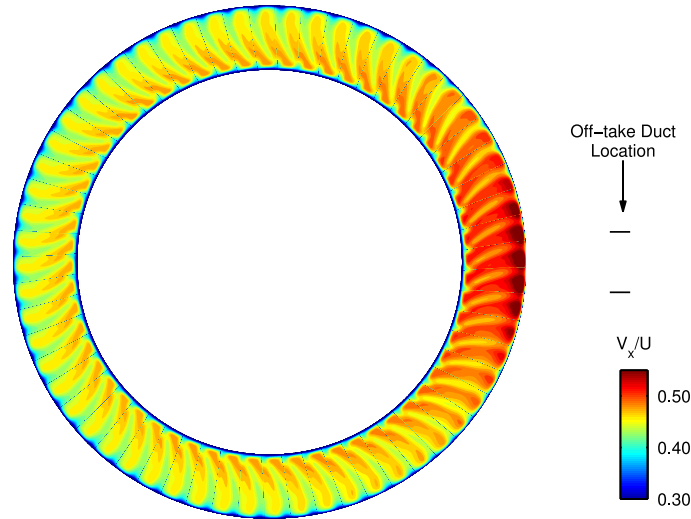


Fig. 4: Upstream of slot, CFD calculated flow field. $\bar{\phi}_{\text{stage}} = 0.43$, bleed rate = 4.2%

Stage inlet

Figures 5 and 2(c) show that at a negative circumferential position relative to the off-take duct, flow coefficient is reduced and at positive circumferential positions relative to the duct, flow coefficient is increased. This asymmetry is driven by the response of the stage to non-uniform inlet flow. The asymmetry is strongest at stage entry and decays with axial distance away from the stage. The circumferential redistribution of the flow varies in the spanwise direction, with greater non-uniformity in the outer 30% of span. Flow angle varies with circumferential position and Fig. 2(c) shows the asymmetric variation in α associated with the static pressure distortion generated by non-uniform bleed. Together, the flow coefficient and absolute flow angle produce a region of reduced passage-averaged relative flow angle with a computed trough 0.49 degrees less than $\bar{\alpha}_{rel}$ while the experimentally measured value is 0.46 degrees. Reducing flow angle in the rotor relative frame increases the rotor incidence and it is this effect which leads to a reduction in compressor operating range with non-uniform bleed.

Downstream of rotor row

The contour plot of flow coefficient in Fig. 6 shows that the flow varies in the circumferential direction but that the change in flow coefficient is more uniform across the span than at stage inlet (see Fig. 5). Figure 7 shows the passage-averaged distribution of stagnation pressure around the annulus at stage inlet and downstream of the rotor. Upstream of the stage the stagnation pressure varies by $\pm 0.7\%$ of dynamic head. Downstream of the rotor the circumferential variation observed is due to the sector with increased stage inlet rotor incidence operating with increased loading and therefore more total-to-total pressure rise is produced.

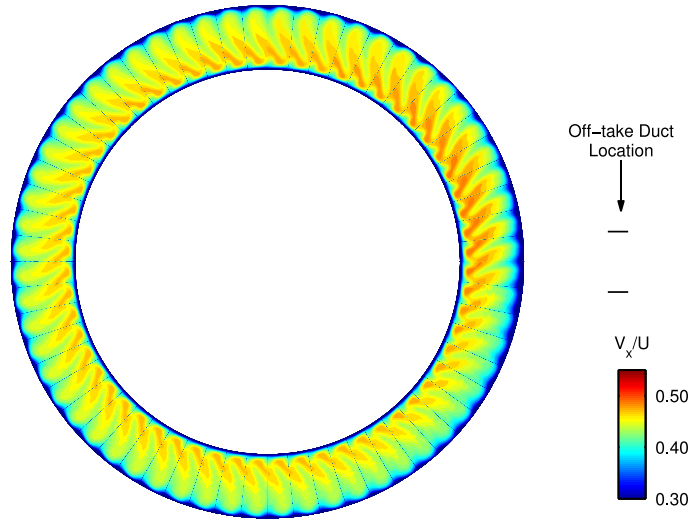


Fig. 5: Stage inlet, CFD calculated flow field. $\bar{\Phi}_{\text{stage}} = 0.43$, bleed rate = 4.2%

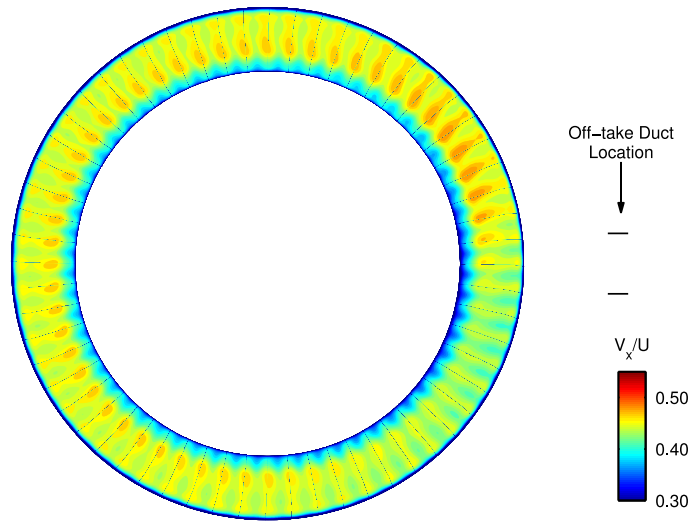


Fig. 6: Downstream of rotor row, CFD calculated flow field. $\bar{\Phi}_{\text{stage}} = 0.43$, bleed rate = 4.2%

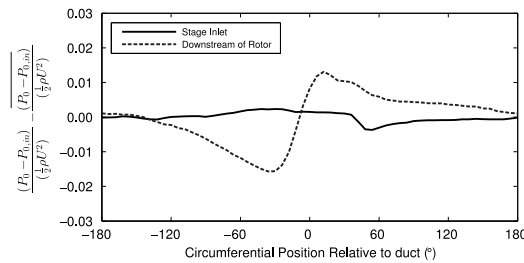


Fig. 7: Passage-averaged distribution of stagnation pressure coefficient at stage inlet and downstream of rotor. $\bar{\Phi}_{\text{stage}} = 0.43$, bleed rate = 4.2%

Downstream of stator row

Figure 8 shows that downstream of the stator row there is circumferential variation in flow coefficient. Close to the circumferential position of the off-take duct, the size of the stator hub corner separation is increased. In the outer 30% of span, flow coefficient is increased due to increased blockage near the hub. The increase in size of the hub corner separation is due to circumferentially non-uniform stator incidence as seen in Fig. 2(d). Downstream of the stator row, Fig. 2(e) shows

that flow angle is circumferentially uniform across the span and the passage-averaged value varies by less than ± 0.2 degrees.

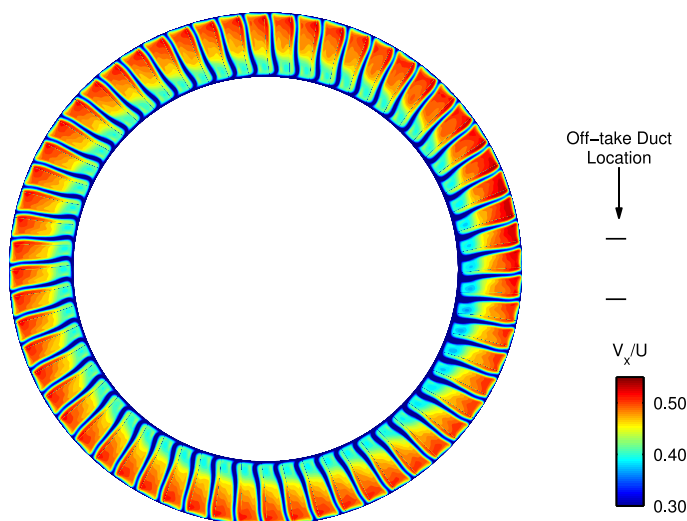


Fig. 8: Downstream of stator row, CFD calculated flow field. $\bar{\Phi}_{\text{stage}} = 0.43$, bleed rate = 4.2%

Bleed system flow

Figure 9 shows computed local bleed rate in the slot at the same location as the local bleed rate is measured in the experimental rig. The width of the peaks are in good agreement, however, the experimental measurements do not have the resolution to capture the maximum local bleed rate.

Figure 10 shows contours of radial velocity coefficient, V_r/U , in the meridional plane at different circumferential locations relative to the off-take duct. Overlaid on the contours are projected streamlines in the same meridional plane. Figure 10(a) shows that -90 degrees away from the off-take duct the bleed slot is almost completely blocked by the separation from the upstream face of the slot. The radial velocity throughout the bleed slot is close to zero. 10 degrees either side of the off-take duct the radial velocity in the bleed slot is high with V_r/U up to 0.60. At the top of the bleed slot two counter rotating vortices are formed; one of these is located in the plenum chamber and the other in the top half of the bleed slot, near the upstream face. Figure 11 shows that these vortices are both drawn into the off-take duct. At the circumferential location of the off-take duct, Fig. 10(c) shows that there is no separation in the bleed slot due to the high local bleed rate. At the inlet to the off-take duct, however, a large separation blocks half of the diameter of the duct causing high radial velocities of up to $V_r/U = 0.80$. This is due to the sharp turning of the flow from the plenum chamber into the off-take duct and is expected to be a region of high loss.

LOW FIDELITY APPROACH: MEAN RADIUS MODEL

The mean radius model serves two purposes. First, it distils the key flow mechanisms and, through their interaction in the model, offers improved insight into the physics of the problem. Second, it provides a far quicker and cheaper method than 3D CFD to study the effect of changes to bleed system and compressor design. We model the flow analytically by coupling a potential flow model for non-uniform bleed extraction with the steady form of the Hynes and Greitzer compressor model [14]. Hynes and Greitzer used their compressor model to study the effect of stagnation pressure inlet distortion

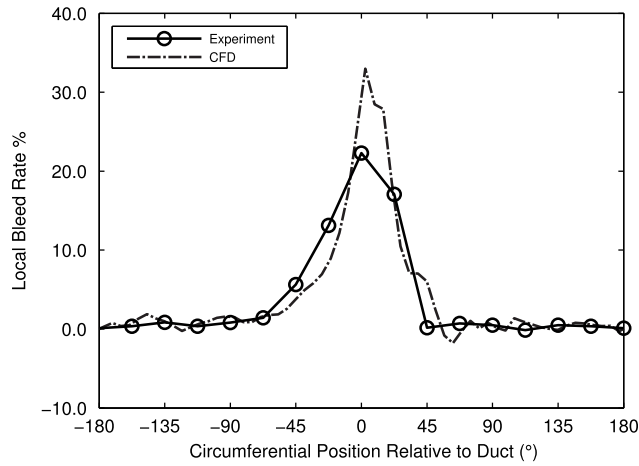


Fig. 9: CFD calculated local bleed rate at 80% of slot height compared with experimental measurements. $\bar{\phi}_{\text{stage}} = 0.43$, bleed rate = 4.2%. The CFD local bleed rate is averaged over 6 degree sections

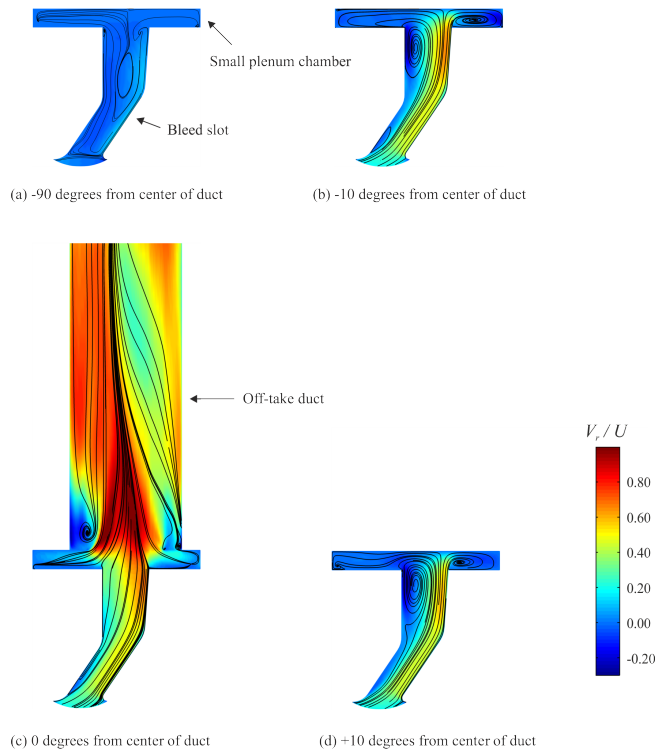


Fig. 10: CFD calculated contours of radial velocity coefficient at different circumferential locations. Overlaid are projected streamlines in the same plane as the contours. $\bar{\phi}_{\text{stage}} = 0.43$, bleed rate = 4.2%.

while Graf et al. [15] adapted it to investigate the effect of non-axisymmetric tip clearance flow. Although in principal a compressible flow mean radius model could be formulated, for simplicity we adopt an incompressible approach for the low speed stage under investigation in the current work.

Methodology

In Grimshaw et al. [7] it is argued that the flow upstream of and through the compressor can be approximated as two-dimensional. This is due to the high hub-to-tip radius ratio typical of mid-to-rear compressor stages and design operating

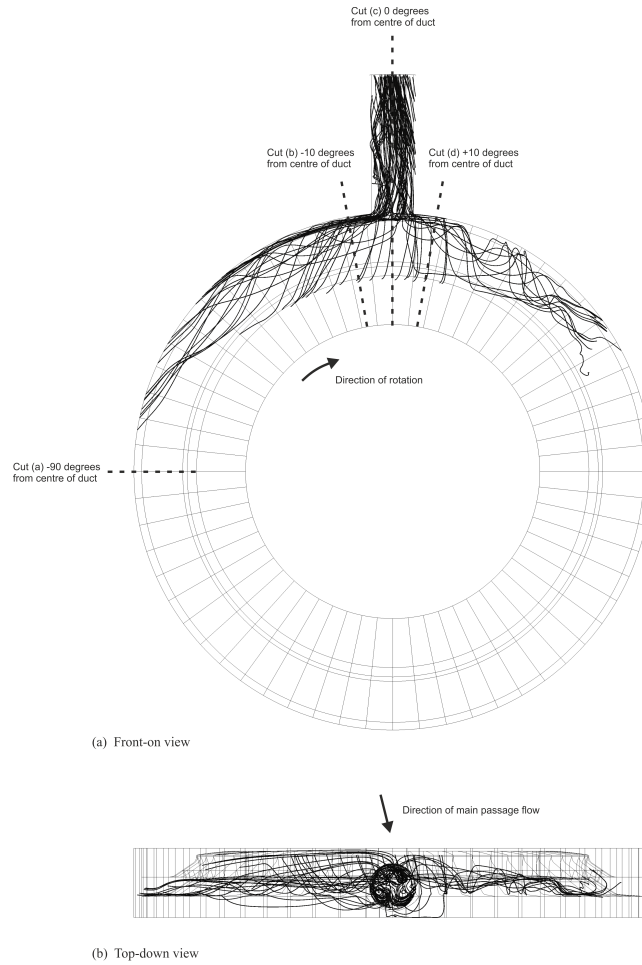


Fig. 11: CFD calculated streamlines in bleed system. Streamlines are seeded in the off-take duct and traced backward towards the plenum chamber and bleed slot. $\bar{\Phi}_{\text{stage}} = 0.43$, bleed rate = 4.2%

point bleed rates of only 1% to 5%. These conditions result in low meridional curvature of the axisymmetric stream surfaces and hence a limited spanwise redistribution of the flow. Experimental data confirm this as a reasonable assumption with three results: stage characteristics for different uniform bleed rates collapse towards one line, the change in spanwise distribution of flow coefficient for different bleed rates is small and compressor performance with non-uniform bleed can be explained in terms of a passage-averaged analysis which ignores spanwise variation [7].

Hynes and Greitzer [14] argue that a major part of the physics of the problem can be obtained through a linear analysis of the upstream and downstream flow fields, coupled to a non-linear compressor model. Specifically, the compressor enters the model as a set of matching conditions for the upstream and downstream flows.

The bleed extraction from the upstream flow is represented as the potential field due to a row of sinks. The circumferential non-uniformities in the potential flow field are then input into the compressor model which in response perturbs the upstream flow. The velocity field due to the compressor matching can then be superposed on the initial potential field to give a new solution for the upstream flow.

The rest of this section provides detailed information on the potential flow and compressor components of the model, and how they are linked and solved.

Potential field

Experiments show that the passage-averaged stagnation pressure at stage inlet varies by only $\pm 0.5\%$ of inlet dynamic head so that the flow upstream of the stage can be modelled as a potential flow. Non-uniform bleed extraction is represented as a row of sinks with non-uniform strength added to a mean axial and circumferential velocity. The distribution of the sink strengths is a model input. It is of a Gaussian form, symmetric about 0° circumferential position and set so that the bleed extraction in the model matches experimental measurements. For a row of S sinks the induced flow is given by the differentiation of the complex potential:

$$V_x - iV_\theta = \frac{dF}{dz} = \sum_{s=1}^S \frac{m(s)}{2\pi \tanh\left(\frac{z - ir_{mid}\theta(s)}{2r_{mid}}\right)} \quad (1)$$

where $m(s)$ is the strength of sink s , x is an axial coordinate in the potential flow field, θ is a circumferential coordinate, $z = x + ir_{mid}\theta$, and $\theta(s)$ is the circumferential location of sink s .

Figure 12 shows the flow coefficient and Fig. 13 the compatible flow angles upstream and downstream of the row of sinks without the downstream stage. The distribution of flow coefficient is symmetric about the mean flow coefficient and the flow angle is asymmetric about the peak bleed location (in this case the mean flow angle is 0°).

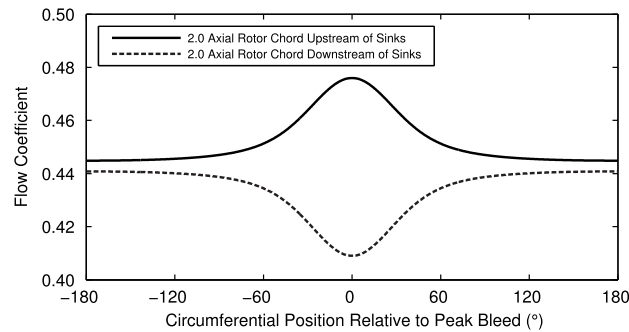


Fig. 12: Flow coefficient upstream and downstream of the row of sinks evaluated from the potential flow model

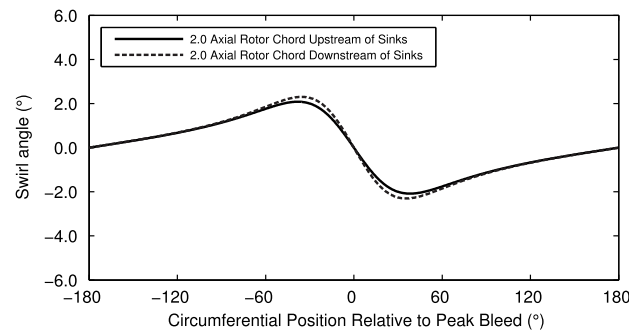


Fig. 13: Flow angle upstream and downstream of the row of sinks evaluated from the potential flow model

Compressor model

The equation for the compressor describes the way in which flow at compressor entry must adjust to satisfy the condition of uniform exit pressure, specifically:

$$\frac{P_2 - P_{01}}{\frac{1}{2}\rho U^2} = \psi(\phi_1, \alpha_1) - \lambda \frac{d\phi_1}{d\theta} \quad (2)$$

where P_2 is exit static pressure, P_{01} is stagnation pressure, ρ is density, U is midspan blade speed, ψ is the non-dimensional stage total-to-static pressure rise with uniform bleed, ϕ_1 is stage inlet flow coefficient, α_1 is stage inlet flow angle in the absolute frame, λ is an inertia term and θ is circumferential location.

The inlet stagnation pressure and exit static pressure are circumferentially uniform so the left hand side of Equation 2 is constant for a given throttle setting. The $\lambda d\phi_1/d\theta$ term represents the acceleration and deceleration of the fluid in the rotor passages as it passes through the changing flow field. This acceleration is balanced by ψ , the local pressure rise which varies around the annulus.

ψ is a function of the local flow coefficient and flow angle. In order to calculate ψ it is linearised so that:

$$\psi(\phi_1, \alpha_1) = \bar{\psi} + \left. \frac{\partial \psi}{\partial \phi_1} \right| \delta \phi_1 + \left. \frac{\partial \psi}{\partial \alpha_1} \right| \delta \alpha_1 \quad (3)$$

$\partial \psi / \partial \phi_1$ is found from the measured stage pressure rise characteristic. If the local flow coefficient is below the stalling flow coefficient an extrapolation is made similar to that shown in [14]. The effect of flow angle on stage pressure rise was not tested on the current rig. However, in Young [16], a similar low-speed, one stage test compressor is tested with different IGV stagger angles. Young's result for $\partial \psi / \partial \alpha_1$ is used in our model, along with the variation in stage inlet flow angle, to find the third term in Equation 3. We also use the inertia term, λ , defined in Hynes and Greitzer [14] as:

$$\lambda = \frac{c_{x,rotor}}{\frac{1}{2}r_{mid} \cos^2 \gamma} \quad (4)$$

where $c_{x,rotor}$ is the midspan rotor axial chord, r_{mid} is the mid-height radius and γ is the rotor blade stagger angle.

Solution procedure

Equation 2 is a first-order differential equation for ϕ_1 and is rearranged to give:

$$\frac{d\phi_1}{d\theta} = \frac{\psi(\phi_1, \alpha_1) - \frac{P_2 - P_{01}}{\frac{1}{2}\rho U^2}}{\lambda} \quad (5)$$

Equation 5 is solved using a Fourier transform approach. In this method the circumferential non-uniformities are defined as:

$$\delta \phi = \phi_1 - \bar{\phi}_1 \quad (6)$$

$$\delta \beta = \beta_1 - \bar{\beta}_1 \quad (7)$$

where ϕ is flow coefficient and β is the circumferential velocity coefficient, i.e. V_θ/U . The non-uniform distributions are then decomposed into components caused by the sinks in the potential flow (i.e. the bleed extraction) and the compressor:

$$\delta\phi = \delta\phi_{\text{bleed}} + \delta\phi_{\text{comp}} \quad (8)$$

$$\delta\beta = \delta\beta_{\text{bleed}} + \delta\beta_{\text{comp}} \quad (9)$$

These variations in flow coefficient and circumferential velocity coefficient are expressed as Fourier series which are linked by the potential flow relationships, e.g.

$$\delta\tilde{\phi}_{\text{comp}} = \sum_{n=-\infty}^{\infty} c_n e^{in\theta + |n| \frac{x-x_{\text{comp}}}{r}} \quad (10)$$

$$\delta\tilde{\beta}_{\text{comp}} = \sum_{n=-\infty}^{\infty} \frac{i|n|}{n} c_n e^{in\theta + |n| \frac{x-x_{\text{comp}}}{r}} \quad (11)$$

where c_n are the Fourier coefficients, θ is the circumferential coordinate, x an axial coordinate and x_{comp} the axial coordinate at stage inlet.

Now differentiating ϕ with respect to θ :

$$FT\left(\frac{d\phi_1}{d\theta}\right) = FT\left(\frac{d(\bar{\phi}_1 + \delta\phi)}{d\theta}\right) = FT\left(\frac{d(\delta\phi)}{d\theta}\right) = in\delta\tilde{\phi} \quad (12)$$

and, combining Equations 5 and 12, gives

$$\delta\tilde{\phi} = FT\left(\frac{\Psi(\phi_1, \beta_1) - \frac{P_2 - P_{01}}{\frac{1}{2}\rho U^2}}{\lambda in}\right) \quad (13)$$

From Equation 13, $\delta\tilde{\beta}$ can be found via the potential flow relationships and both $\delta\phi$ and $\delta\beta$ recovered by inverting the Fourier transforms. Finally, ϕ_1 and β_1 are calculated from Equations 6 and 7.

This set of equations are solved iteratively. The initial guess for ϕ and β are taken from the potential flow field at the axial location of stage inlet. Equation 13 is evaluated and this leads to a new estimate for ϕ . ϕ is updated using this estimate and a suitable relaxation parameter. The calculation is converged when the change in ϕ from one step to the next is small, i.e. less than 5×10^{-5} at all circumferential locations. Once the compressor calculation has converged the velocity perturbation due to the compressor can be found from Equation 8. This velocity perturbation decays upstream of the stage and is added to the velocity field from the potential flow.

The axial distance between the row of sinks and compressor model (i.e. where the compressor velocity perturbation is applied to the upstream flow) is set to match the distance between the bleed slot and stage inlet in the experiment. The planes at which the model outputs are taken, upstream of the bleed slot and at stage inlet, are set to the same location as the measurement planes in the rig tests.

The solution converges in approximately 50 steps and this takes around 10 seconds on a laptop PC.

Results

Figures 14 and 15 show the flow distribution around the annulus upstream of the bleed slot for $\bar{\phi}_{\text{stage}} = 0.43$ and $\bar{\phi}_{\text{stage}} = 0.38$. The model predictions for flow coefficient are predicted to within 0.01 (2.5% of $\bar{\phi}$). The shape of the distributions also match the rig data well. At this location the static pressure field associated with the non-uniform bleed extraction dominates and the influence of the compressor stage is less strong. This can be seen in that the flow distributions upstream of the bleed slot do not change significantly as the compressor is throttled.

At stage inlet (downstream of bleed slot) with $\bar{\phi}_{\text{stage}} = 0.43$ and $\bar{\phi}_{\text{stage}} = 0.38$, Figs. 16 and 17 show that the model continues to match the experimental measurements quite well. At $\bar{\phi}_{\text{stage}} = 0.43$ the flow coefficient is within 0.015 (3.5% of $\bar{\phi}$) of rig data and at $\bar{\phi}_{\text{stage}} = 0.38$ the flow coefficient is within 0.005 (1.3% of $\bar{\phi}$). At this location the flow is affected by non-uniform bleed extraction and the upstream effect of the compressor stage. This interaction can be seen most clearly in Figs. 16(a) and 17(a) where the shape of the flow coefficient distribution at stage inlet changes as the operating point is varied. The figures also show that the model is able to reproduce this change in shape.

The model absolute flow angle distributions upstream of the bleed slot (shown in Figs. 14(b) and 15(b)) match the experimental results to within 1° . However at stage inlet (Figs. 16b and 17b) the predictions are less good, with the model over-predicting the flow angle by up to 4° , twice the passage-averaged experimental measurement. The reason for this is the assumption of two-dimensional flow. Figure 18(a) shows that upstream of the bleed slot the measured change in spanwise variation in absolute flow angle, around the annulus, is small, so the assumption of two-dimensional flow is reasonable. However, Fig. 18(b) shows that downstream of the bleed slot, the variation in flow angle around the annulus changes significantly with span, especially above 70% passage height. This is due to the decay, in the spanwise direction, of the static pressure field associated with non-uniform bleed extraction. Our two-dimensional model does not capture this effect and hence there is an over-prediction (compared to passage-averaged test results) of the variation in absolute flow angle. A result of this is that the variation in relative flow angle (and hence rotor incidence) at stage inlet is also over-predicted compared to passage-averaged experimental data.

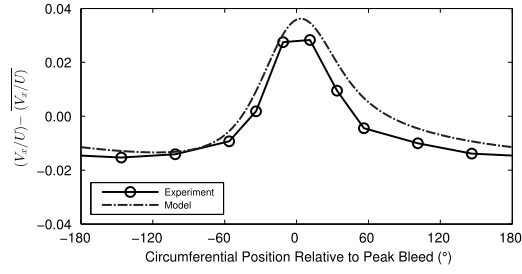
Sensitivity analysis

The key inputs for the compressor model are the pressure rise response to stage inlet flow coefficient and flow angle, and the inertia term, λ . $\partial\psi/\partial\phi_1$ and $\partial\psi/\partial\alpha_1$ are taken from experimental results, while λ is based on simple 1D analysis (not measured data). The sensitivity of the model to changes in these terms is now assessed.

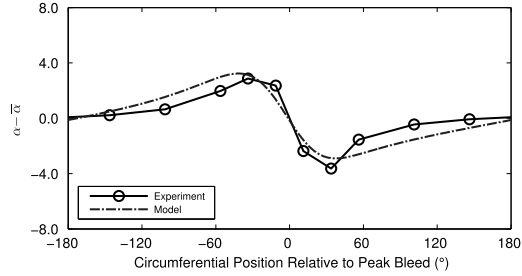
The λ term used for the model (Equation 4) is dependent only on geometric features of the compressor. Chue et al. [17] proposed an additional term for λ to account for unsteady rotor losses, so that:

$$\lambda = \frac{c_x}{\frac{1}{2}r\cos^2\gamma} - \frac{c_x}{r\phi} \left[\frac{d\psi}{d\phi} \Big|_{\text{ideal}} - \frac{d\psi}{d\phi} \Big|_{\text{real}} \right] \quad (14)$$

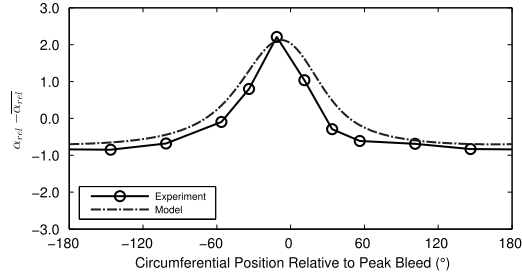
The ideal gradient of the pressure rise characteristic can be estimated by fitting a line through the measured characteristic at the design operating point. Figure 19 shows the effect of using the Chue et al. model for λ . At $\bar{\phi}_{\text{stage}} = 0.38$ the variation in flow coefficient distribution at stage inlet, using the different models, is less than 0.001. At $\bar{\phi}_{\text{stage}} = 0.43$ the maximum



(a) Distribution of flow coefficient, ϕ



(b) Distribution of absolute flow angle, α

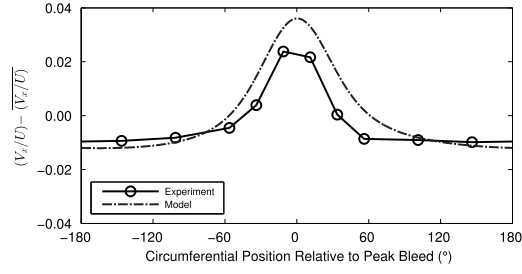


(c) Distribution of relative flow angle, α_{rel}

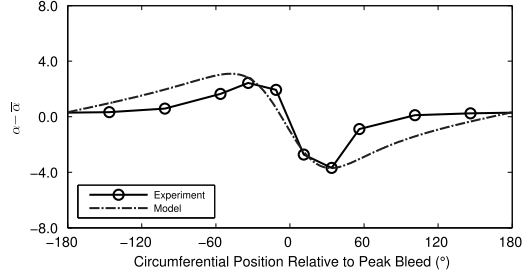
Fig. 14: Comparison of passage-averaged experimental data and model output upstream of bleed slot, $\bar{\phi}_{stage} = 0.43$

variation increases slightly to 0.003, though this is a change of only 0.6% of the mean flow coefficient. We conclude that the sensitivity of the model to changes in λ is small.

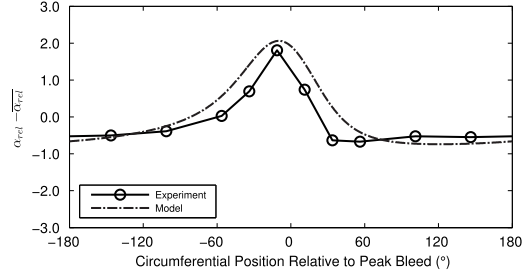
To investigate the sensitivity of the model to ψ we rerun the model with the second and then the third term in Equation 3 removed. The results of these changes are shown in Fig. 20. At stage inlet, for $\bar{\phi}_{stage} = 0.43$, Fig. 20(a) shows that removing the $\partial\psi/\partial\alpha_1 \delta\alpha_1$ term causes the flow coefficient distribution to lose its asymmetric shape, i.e. the asymmetry was being generated by the pressure rise response to the asymmetric flow angle. Removing the $\partial\psi/\partial\phi_1 \delta\phi_1$ term results in a large region of reduced flow coefficient which is driven primarily by the non-uniform bleed extraction, c.f. Fig. 12 which shows the flow coefficient distribution with no downstream stage. Without the response to flow coefficient, the compressor stage has much less influence on the upstream flow. At $\bar{\phi}_{stage} = 0.38$ the sensitivity of the solution to the removal of each term is reduced. This is because both terms are smaller: the gradient of the measured pressure rise characteristic reduces as the compressor is throttled and the change in pressure rise with flow angle approaches zero for flow coefficients close to stall. In conclusion, the coupling of the downstream stage with non-uniform bleed extraction is sensitive to the response of both the stage inlet flow coefficient and flow angle.



(a) Distribution of flow coefficient, ϕ



(b) Distribution of absolute flow angle, α



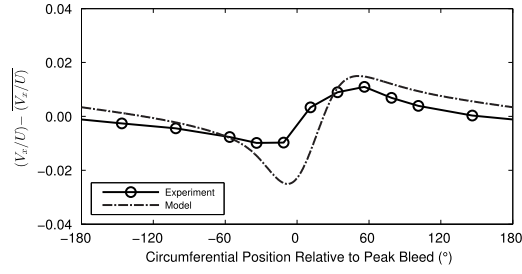
(c) Distribution of relative flow angle, α_{rel}

Fig. 15: Comparison of passage-averaged experimental data and model output upstream of bleed slot, $\bar{\phi}_{stage} = 0.38$

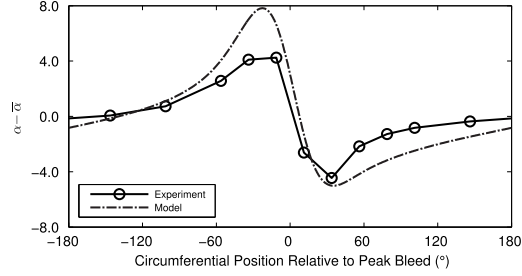
Design Changes

The mean radius model allows the investigation of the effect of changes that may be considered while designing the bleed system and its integration with the compressor; here we consider two examples.

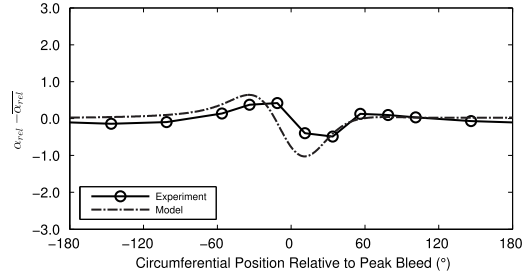
Increasing the size of the plenum chamber and increasing the number of off-take ducts reduces the non-uniformity of the bleed extraction. In our model this means changing the sink strength distribution $m(s)$ in Equation 1. In addition to the original distribution, two further Gaussian distributions, with the same overall bleed rate of 4.1%, have been applied to the model. These distributions are based on experimental measurements taken in [7] however this data is unlikely to be available for preliminary design studies. Instead, a coarse mesh CFD computation including the annulus (without blades to reduce mesh size), bleed slot, plenum chamber and off-take duct boundary condition can be used to predict the bleed extraction for different numbers of ducts and sizes of plenum chamber. This can then be used to set the sink strength distribution. The local bleed extraction rates for the three distributions are shown in Fig. 21(a); Fig. 21(b) shows their effect on the stage inlet relative flow angle, at $\bar{\phi}_{stage} = 0.38$. As expected, the case with reduced bleed non-uniformity, representative of a bleed system with a larger plenum chamber and with a peak bleed rate of 4.9%, reduces the circumferential variation in relative flow angle to less than 0.1° at stage inlet.



(a) Distribution of flow coefficient, ϕ



(b) Distribution of absolute flow angle, α



(c) Distribution of relative flow angle, α_{rel}

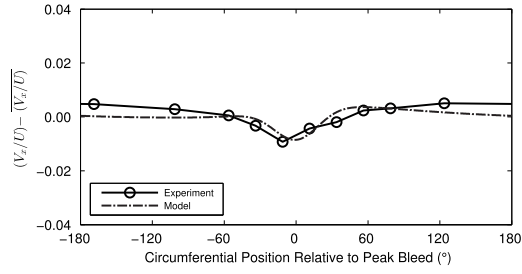
Fig. 16: Comparison of passage-averaged experimental data and model output downstream of bleed slot, $\bar{\Phi}_{stage} = 0.43$

Another design consideration is how close a downstream stage should be located to the bleed slot and this is easily assessed using the mean radius model. Here, the compressor stage is moved from $0.8C_{x,rotor}$ to $1.6C_{x,rotor}$ and $2.4C_{x,rotor}$ downstream of the bleed slot, while the plane at which the results are extracted is fixed at $0.2C_{x,rotor}$ upstream of the stage. Figure 22 shows that non-uniformity of the stage inlet flow reduces as the stage is moved away from the slot. This is because the influence of the bleed extraction decays downstream of the sinks and its perturbation on the flow and the perturbation from the compressor caused by the non-uniform flow, are reduced.

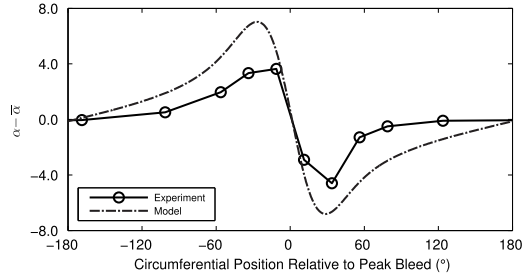
CONCLUSIONS

The following conclusions are drawn from the current work:

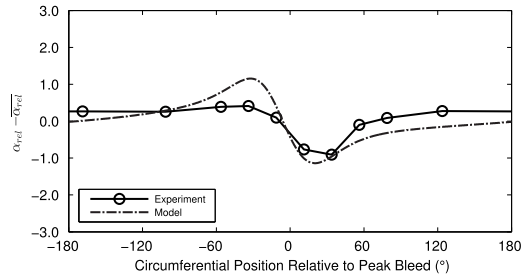
1. The performance of a compressor with non-uniform bleed has been accurately simulated using a full annulus and bleed system URANS computation. Circumferential distributions of flow coefficient and flow angle agree with experimental data to within 0.005 and 0.5 degrees respectively.
2. A simplified mean radius model has been developed and shown to reproduce the key features of the flow provided that



(a) Distribution of flow coefficient, ϕ



(b) Distribution of absolute flow angle, α



(c) Distribution of relative flow angle, α_{rel}

Fig. 17: Comparison of passage-averaged experimental data and model output downstream of bleed slot, $\bar{\phi}_{stage} = 0.38$

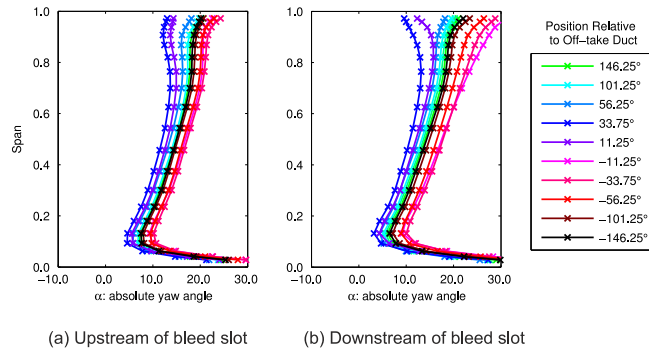
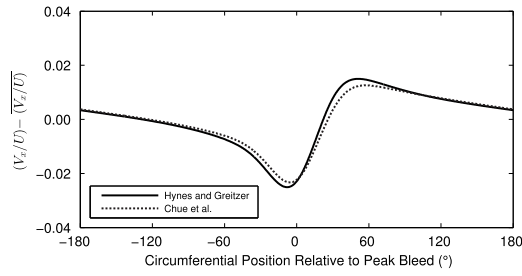


Fig. 18: Measured spanwise distributions of flow angle at different circumferential locations, $\bar{\phi}_{stage} = 0.43$

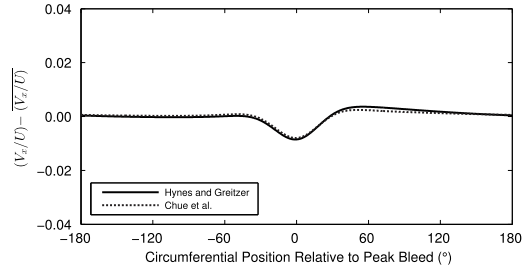
the clean flow pressure rise characteristic of the compressor is known *a priori*.

3. We interpret the agreement between the results of the mean radius model and the measured data to mean that the key features to be accounted for in compressor-bleed interaction are:

- (a) the one-dimensional compressor performance via the pressure rise characteristic as a function of both flow coefficient and inlet swirl;

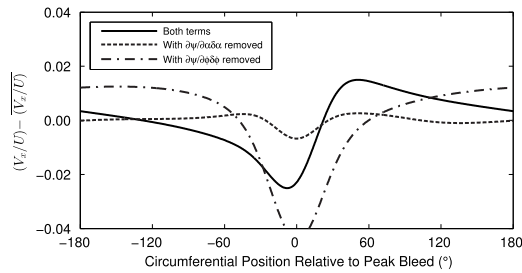


(a) $\bar{\Phi}_{stage} = 0.43$

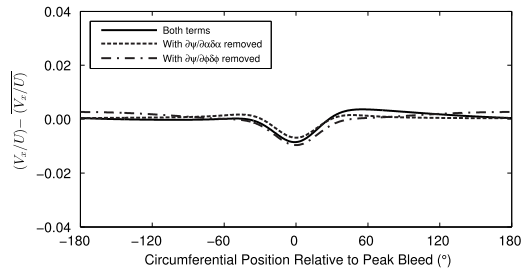


(b) $\bar{\Phi}_{stage} = 0.38$

Fig. 19: Distribution of flow coefficient at stage inlet with different models for λ



(a) $\bar{\Phi}_{stage} = 0.43$

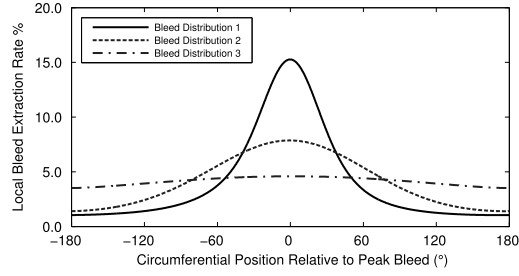


(b) $\bar{\Phi}_{stage} = 0.38$

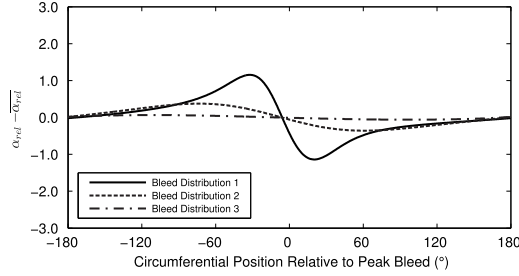
Fig. 20: Distribution of flow coefficient at stage inlet with modifications to ψ

- (b) the unsteady response of the compressor to the circumferentially non-uniform inlet flow via the inertia term λ ;
- (c) the flow redistribution ahead of the compressor, driven jointly by the bleed and by the compressor response.

4. The compressor acts to flatten the flow non-uniformity induced by the bleed extraction and the compressor sensitivity to inlet swirl introduces an asymmetric component to the flow distribution at stage inlet.
5. The mean radius model allows the rapid assessment of the bleed system design prior to down-selection for detailed



(a) Local bleed extraction rate, %



(b) Distribution of relative flow angle, α_{rel}

Fig. 21: Relative flow angle distributions at stage inlet for different levels of bleed non-uniformity, $\bar{\Phi}_{stage} = 0.38$

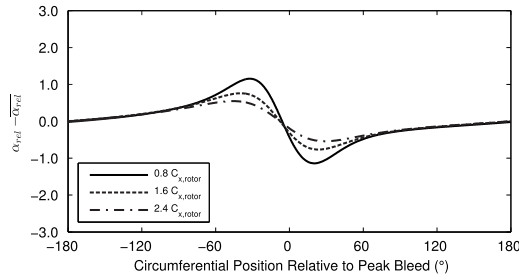


Fig. 22: Relative flow angle distributions at stage inlet with different axial spacing between bleed and stage, $\bar{\Phi}_{stage} = 0.38$

analysis using full 3D (unsteady) computations.

ACKNOWLEDGEMENTS

The authors are grateful for the comments and suggestions made by members of the Whittle Laboratory, the Gas Turbine Lab at MIT, and Mitsubishi Heavy Industries who have provided assistance during the course of the project: Dr. A.M. Young, Mr. J.V. Taylor, Professor E.M. Greitzer, Professor Z.S. Spakovszky, Dr. S. Aoki, Dr. S. Uchida, Dr. E. Ito, Mr. T. Walker and Mr. R. Mito.

NOMENCLATURE

$c_{x,rotor}$	Rotor midspan axial chord
r_{mid}	Mid-height radius
γ	Rotor blade stagger angle
P	Pressure
P_0	Stagnation pressure
U	Mid-height blade speed
V_x	Axial velocity
V_θ	Circumferential velocity
V_r	Radial velocity
α	Flow angle
α_{rel}	Relative flow angle
ρ	Density
ϕ	Flow coefficient = V_x/U
β	Circumferential velocity coefficient = V_θ/U
ψ	Total-to-static pressure rise coefficient = $\frac{P_2 - P_{01}}{\frac{1}{2}\rho U^2}$
λ	Inertia parameter
θ	Circumferential location
x	Axial location
$[]_{in}$	At rig inlet
$[]_1$	At stage inlet
$[]_2$	At stage exit
$\bar{[]}$	Mean value
$\tilde{[]}$ or $FT([])$	Fourier transformed

References

- [1] Conan, F. and Savarese, S., 2001. "Bleed Airflow CFD Modelling in Aerodynamics Simulations of Jet Engine Compressors". *ASME IGTI Turbo Expo, 2001-GT-544*.
- [2] Wellborn, S.R. and Koiro, M., 2002. "Bleed Flow Interactions with an Axial Flow Compressor Powerstream". *AIAA/ASME Joint Propulsion Conference, AIAA 2002-4057*.
- [3] Di Mare, L. and Simpson, G. and Mueck, B. and Sayma, A., 2006. "Effect of Bleed Flows on Flutter and Forced Response of Core Compressors". *ASME IGTI Turbo Expo, GT2006-90683*.
- [4] Leishman, B.A. and Cumpsty, N.A. and Denton, J.D., 2007. "Effects of Bleed Rate and Endwall Location on the Aerodynamic Behavior of a Circular Hole Bleed Off-Take". *ASME J. Turbomach.*, **129**.
- [5] Leishman, B.A. and Cumpsty, N.A. and Denton, J.D., 2007. "Effects of Inlet Ramp Surfaces on the Aerodynamic Behavior of Bleed Hole and Bleed Slot Off-Take Configurations". *ASME J. Turbomach.*, **129**.

- [6] Leishman, B.A. and Cumpsty, N.A., 2007. "Mechanism of the Interaction of a Ramped Bleed Slot With the Primary Flow". *ASME J. Turbomach.*, **129**.
- [7] Grimshaw, S.D. and Pullan, G. and Walker, T., 2015. "Bleed-induced Distortion in Axial Compressors". *ASME J. Turbomach.*, **137**.
- [8] Gomes, R. and Schwarz, C. and Peitzner, M., 2005. "Aerodynamic Investigations of a Compressor Bleed Air Configuration Typical for Aeroengines". *ISABE-2005-1264*.
- [9] Gomes, R. and Schwarz, C., 2006. "Experimental Investigation of a Generic Compressor Bleed System". *ASME IGTI Turbo Expo, GT2006-90458*.
- [10] Reid, C., 1969. "The Response of Axial Flow Compressors to Intake Flow Distortion". *ASME 69-GT-29*.
- [11] Rosic, B.R. and Mazzone, C.M. and Bignell, Z., 2014. "Aerodynamic Analysis of Steam Turbine Feed-Heating Steam Extractions". *ASME J. Turbomach.*, **136**.
- [12] Gunn, E.J. and Hall, C.A., 2014. "Aerodynamics of Boundary Layer Ingesting Fans". *ASME IGTI Turbo Expo, GT2014-26142*.
- [13] Brandvik, T. and Pullan, G., 2011. "An Accelerated 3D Navier-Stokes Solver for Flows in Turbomachines" *ASME J. Turbomach.*, **133**.
- [14] Hynes, T.P. and Greitzer, E.M., 1987. "A Method for Assessing Effects of Circumferential Flow Distortion on Compressor Stability" *ASME J. Turbomach.*, **109**.
- [15] Graf, M.B. and Wong, T.S. and Greitzer, E.M. and Marble, F.E. and Tan, C.S. and Shin, H.W. and Wisler, D.C., 1998. "Effects of Nonaxisymmetric Tip Clearance on Axial Compressor Performance and Stability" *ASME J. Turbomach.*, **120**.
- [16] Young, A.M., 2012. "Tip-Clearance Effects in Axial Compressors" *University of Cambridge*.
- [17] Chue, R. and Hynes, T.P. and Greitzer, E.M. and Tan, C.S. and Longley, J.P., 1989. "Calculations of Inlet Distortion Induced Compressor Flow Field Instability" *Int. J. Heat and Fluid Flow*, **10**.